ChemComm

Actinide Arene-Metalates: 2. A Neutral Uranium Bis(Anthracenide) Sandwich Complex and Elucidation of its Electronic Structure

Journal:	*ChemComm*
Manuscript ID	CC-COM-06-2022-003238.R1
Article Type:	Communication

COMMUNICATION

Actinide arene-metalates: 2. A neutral uranium bis(anthracenide) sandwich complex and elucidation of its electronic structure

Received 00th January 20xx,
Accepted 00th January 20xx

DOI: 10.1039/x0xx00000x

Jesse Murillo,[a] Rina Bhowmick,[b] Katie L. M. Harriman,[c] Alejandra Gomez-Torres,[a] Joshua Wright,[d] Pere Miró,[b] Alejandro Metta-Magaña,[a] Muralee Murugesu,[c] Bess Vlaisavljevich,*[,b] and Skye Fortier*[,a]

An unprecedented sandwich complex of the actinides is synthesized from the treatment of $[UI_2(HMPA)_4]I$ (HMPA = $OP(NMe_2)_3$) (2) with 3 equiv. of $K[C_{14}H_{10}]$ to give the neutral, bis(arenide) species $U(\eta^6\text{-}C_{14}H_{10})(\eta^4\text{-}C_{14}H_{10})(HMPA)_2$ (1). Solid-state X-ray, SQUID magnetometry, and XANES analyses are consistent with tetravalent uranium supported by $(C_{14}H_{10})^{2-}$ ligands. In one case, treatment of 1 with an equiv. of AgOTf led to the isolation of $U(\eta^6\text{-}C_{14}H_{10})_2(HMPA)(THF)$ (3), formed from ring migration and haptotropic rearrangement. Complete active space (CASSCF) calculations indicate the U-C bonding to solely consist of π-interactions, presenting a unique electronic structure distinct from classic actinide sandwich compounds.

The sandwich compounds ferrocene, Cp_2Fe (Cp = C_5H_5), and bis(benzene)chromium(0), $(\eta^6\text{-}C_6H_6)_2Cr$, heralded in a new golden era of organometallic chemistry.[1] These compounds changed the chemical landscape by revealing unprecedented bonding-modes between metals and carbon. In the case of transition metals, electronic structure analysis has revealed a key role of the metal *d*-orbitals in the bonding scheme of sandwich-type molecules. For instance, in $(\eta^6\text{-}C_6H_6)_2Cr$, δ-backbonding to benzene π*-orbitals has been shown to be a major contributor to its molecular orbital picture.[2] With regards to organic chemistry, metal-coordination to an aromatic ring alters its electronic character, facilitating nucleophilic additions and providing other pathways for the derivatization of aromatic hydrocarbons.[3]

Arene sandwich complexes of the *f*-elements remain rare but are important for understanding the metal valence orbital contributions to chemical bonding. In the case of the lanthanides, only the 1,3,5-tri-*tert*-butylbenzene derivatives $Ln(\eta^6\text{-}^tBu_3C_6H_3)_2$ (Ln = La, Pr, Nd, Sm, Gd, Tb, Dy, Ho, Er, and Lu) have been isolated, requiring electron-beam vaporization techniques for their syntheses.[4] Nevertheless, the trinuclear sandwich complex, $[K([2.2.2]\text{-cryptand})]_2\{[(KL_3Ce)(\mu\text{-}\eta^6\text{:}\eta^6\text{-}C_7H_8)]_2Ce\}$ (L = $^-OSi(O^tBu)_3$), featuring a $[Ce(\eta^6\text{-}C_7H_8)_2]^{2-}$ core, was reported in 2017.[5] With respect to the actinides, uranium-arene bonding is predicted to be thermodynamically favourable; however, attempts to synthesize homoleptic arene-sandwich complexes have been unsuccessful over the years.[6]

Recently, we reported the first structurally characterized examples of uranium arene-metalate sandwich complexes in the form of the methoxy-bridged bis(anthracenide) uranium dimers $[K(18\text{-crown-6})(THF)_2]_2[U(\eta^6\text{-}C_{14}H_{10})(\eta^4\text{-}C_{14}H_{10})(\mu\text{-}OMe)]_2\square 4THF$ (**A^{18C6}**) and $\{[K(THF)_3][U(\eta^6\text{-}C_{14}H_{10})(\eta^4\text{-}C_{14}H_{10})(\mu\text{-}OMe)]\}_2$ (**A^{THF}**).[7] Compounds **A^{18C6}** and **A^{THF}** were thoroughly characterized by structural, magnetic, and electronic methods. CASSCF calculations revealed the uranium-arenide interactions to consist of highly polarized π-type bonds with contributions primarily from the uranium 6*d*-orbital manifold. This is surprising as actinide inverted sandwich complexes typically display significant 5*f*-orbital δ-type participation.[8]

In our continuing efforts to synthesize and study unsupported arene-sandwich molecules of the actinide elements, we have targeted the isolation of a mononuclear species, free of confounding interactions provided by counter-ions and bridging ligand contacts as found in **A^{18C6}** and **A^{THF}**. Herein, we report the isolation of the mononuclear sandwich species $U(\eta^6\text{-}C_{14}H_{10})(\eta^4\text{-}C_{14}H_{10})(HMPA)_2$ (HMPA = $OP(NMe_2)_3$) (**1**), generated from the reaction of $K(C_{14}H_{10})$ with the uranium(III) HMPA-solvate *trans*-$[UI_2(HMPA)_4]I$ (**2**). Interestingly, in one case, attempts to oxidize **1** instead led to the unexpected formation of the bis(anthracenide) sandwich $U(\eta^6\text{-}C_{14}H_{10})_2(HMPA)(THF)$ (**3**), a result of anthracene ring migration. The solid-state molecular structures of **1** and **3** are presented, and an electronic structure analysis of both are provided. Moreover, the electronic properties of **1** have been further characterized by magnetic measurements and X-ray absorption near-edge spectroscopy (XANES) analysis.

We reasoned that addition of strongly coordinating HMPA would assist in the synthesis of a mononuclear species, disfavouring the formation of bridging compounds. Ellis and co-workers showed that the tris(naphthalenide) zirconium

[a]*Department of Chemistry and Biochemistry, University of Texas at El Paso, El Paso, Texas 79968, United States*
[b]*Department of Chemistry, University of South Dakota, Vermillion, South Dakota 57069, United States*
[c]*Department of Chemistry and Biomolecular Sciences, University of Ottawa, Ottawa, Ontario K1N 6N5, Canada*
[d] *Department of Physics, Illinois Institute of Technology, Chicago, IL, 60616, United States*
† Electronic Supplementary Information (ESI) available: CCDC 2172188 – 2172190. For ESI see DOI: 10.1039/x0xx00000x

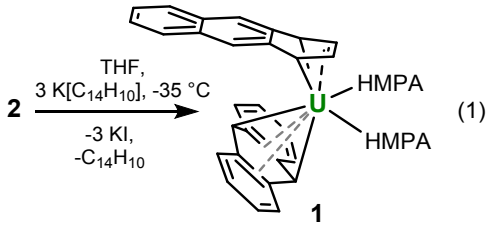

(1)

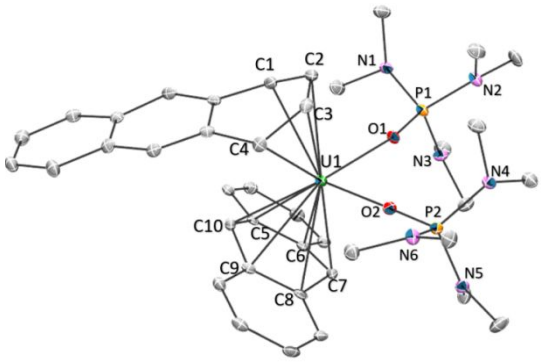

Fig. 1 ORTEP diagram of **1**·THF with 30% thermal probability ellipsoids. Hydrogen atoms and co-crystallized THF are omitted for clarity.

complex [K([2.2.2]-cryptand)]$_2$[Zr(η^4-$C_{10}H_8$)$_3$] is stable in HMPA and can be crystallized from its solutions.[9] In our case, we found the use of HMPA as a co-solvent to be problematic as it was difficult to remove and failed to give tractable solids. Instead, treating UI_3(dioxane)$_{1.5}$ with 4 equiv. of HMPA produces the HMPA-solvate **2** in 94% yield as a deeply blue coloured product.

Addition of **2** to a cold (-35 °C), stirring THF solution containing 3 equiv. of *in-situ* prepared K[$C_{14}H_{10}$] gives rise to a deep purple solution concomitant with the formation of a white precipitate. Filtration of the solution and storage at -35 °C for 24 h affords dark blue, block shaped crystals of **1**·THF in 65% yield [Eq (1)].

Complex **1**·THF is sparingly soluble in THF, which is a slight improvement over the insolubility of $\mathbf{A}^{\mathbf{18C6}}$ and $\mathbf{A}^{\mathbf{THF}}$ in all solvents. The ^{1}H NMR spectrum of **1**·THF in THF-d_8 exhibits two broad signals centred at 12.6 ppm and -46.0 ppm in an 8 to 12 ratio, suggesting equivalence of the two rings on the NMR time scale, with the signal attributable to HMPA appearing at 2.56 ppm (Fig. S7, ESI†). The ^{31}P{^{1}H} NMR spectrum features a weak signal at 87.2 ppm (Fig. S9), which is significantly shifted from the ^{31}P{^{1}H} peak observed for compound **2** (24.6 ppm) (Fig. S6). The UV-Vis of freshly prepared THF solutions of **1** (Fig. S10) is qualitatively similar to that of anthracene, but completely unlike that of [$C_{10}H_{14}$]$^-$.[10] The spectral features may be due to decomposition. Indeed, **1** slowly decomposes in room temperature THF solutions, gradually turning from deep purple to red in colour with formation of 9,10-dihydroanthracene and anthracene with a minor paramagnetic species as the only observable products by ^{1}H NMR spectroscopy after several days (Fig. S8).

The solid-state molecular structure of **1**·THF is shown in Fig. 1. Notably, the anthracenide ligands adopt mixed binding modes identical to that seen in $\mathbf{A}^{\mathbf{18C6}}$ and $\mathbf{A}^{\mathbf{THF}}$, sandwiching the uranium atom between the η^4-$C_{14}H_{10}$ and η^6-$C_{14}H_{10}$ rings with a centroid-uranium-centroid angle of 132.8°, comparable to that found for $\mathbf{A}^{\mathbf{18C6}}$ (C_{cent}-U-C_{cent} = 134.6°) and $\mathbf{A}^{\mathbf{THF}}$ (C_{cent}-U-C_{cent} = 133.4°). In comparison to the bis(naphthalenide)thorium compound {[O-2,4-^{t}Bu$_2$-C_6H_2(CH_2)]$_2$Th(η^4-$C_{10}H_8$)$_2$}$^{2-}$ (C_{cent}-Th-C_{cent} =112.6°),[11] the bend angle between the two anthracenides of **1** is significantly more obtuse. Furthermore, both anthracenide ligands are puckered, displaying a fold angle of 19.6° for η^6-$C_{14}H_{10}$, and a bend angle of 24.1° for η^4-$C_{14}H_{10}$ (Fig. S4), within the range of that seen in $\mathbf{A}^{\mathbf{18C6}}$ (η^6-$C_{14}H_{10}$: 18.8°; η^4-$C_{14}H_{10}$: 26.8°). The U-C distances in **1** (U1-C(η^6-$C_{14}H_{10}$) = 2.546(4) – 2.857(3) Å, avg. 2.72 Å, U-C_{cent} = 2.32 Å; U1-C(η^4-$C_{14}H_{10}$) = 2.662(4) – 2.672(4) Å, avg. 2.67 Å, U-C_{cent} = 2.35 Å) and anthracene C-C bond lengths (Fig. S2) in **1**·THF are comparable to the corresponding bonds in $\mathbf{A}^{\mathbf{18C6}}$.

Determination of the formal oxidation state assignments of the uranium centres in $\mathbf{A}^{\mathbf{18C6}}$ and $\mathbf{A}^{\mathbf{THF}}$ proved to be non-trivial due to the redox non-innocence of anthracene and the redox variability of the central metals. Thorough structural, spectroscopic, and computational analyses indicate that $\mathbf{A}^{\mathbf{18C6}}$ and $\mathbf{A}^{\mathbf{THF}}$ are best described as possessing tetravalent uranium. Based upon structural parameters alone, the comparable bond metrics of the anthracenide ligands between **1**·THF, $\mathbf{A}^{\mathbf{18C6}}$, and $\mathbf{A}^{\mathbf{THF}}$ supports a [$C_{14}H_{10}$]$^{2-}$ assignment for each arenide in the former, therefore suggesting the presence of U(IV) in **1**·THF.

For further elucidation, the solid-state magnetic properties of **1**·THF were measured through SQUID magnetometry. The magnetization plot (Fig. S15) shows an effective magnetic moment of μ_{eff} = 2.31 μ_B at 300 K at 0.1 T that gradually curves to 0.42 μ_B at 1.8 K. The decrease in the μ_{eff} with decreasing temperature can be explained by the thermal depopulation of the metal excited states, which approaches a near-zero value at 1.8 K that is consistent with the singlet ground state of a 5f^2 U^{4+} ion. The room temperature μ_{eff} of **1** is lower than the 3.58 μ_B calculated for a 5f^2 $^3H_4$ ion but is near the average magnetic moment of 2.77 μ_B for U(IV) complexes.[12] Furthermore, the μ_{eff} of **1**·THF at 300 K is close to that found for $\mathbf{A}^{\mathbf{18C6}}$ (μ_{eff} = 2.20 μ_B per uranium ion with non-interacting spins).

To provide a more definitive oxidation state assignment, U L_{III}-edge XANES measurements were performed on a solid, pulverized sample of **1** diluted in a boron nitride matrix and compared against a series of U(III)-U(VI) standards.[13] The normalized L_{III} absorption edge energy for **1** is 17162.4 eV, which is comparable to the 17161.6 eV we found for UCl_4 (Fig. 3 and Table S2). This reinforces a formal U(IV) assignment for the uranium in **1**. In line with this, the absorption edge energy of **1** is in-between $\mathbf{A}^{\mathbf{18C6}}$ (17161.7 eV) and $\mathbf{A}^{\mathbf{THF}}$ (17162.6 eV).

Given the slight solubility of **1** in THF, preliminary attempts to explore its redox chemistry were undertaken. Efforts to reduce **1**·THF using KC_8 or K^0 were unsuccessful. In one case, addition of 1 equiv of AgOTf to **1**·THF in THF at -35 °C was performed, changing from a deep blue mixture to a red-purple solution to give burgundy-coloured crystals upon workup. X-ray crystallographic analysis revealed the formation of **3**·THF·C_6H_{14} (Fig. 4), formed from replacement of an HMPA ligand with a molecule of THF accompanied by anthracene ring migration.

The role of the AgOTf in this transformation is unclear. The

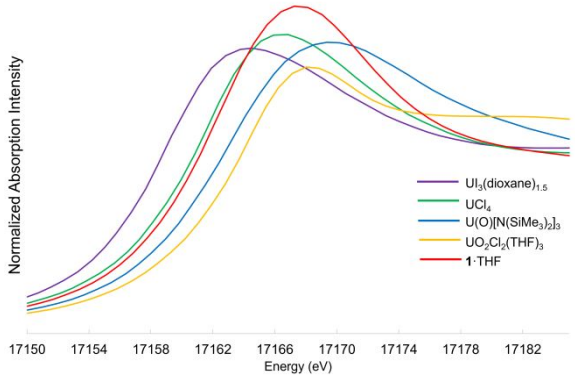

Fig. 3 XANES plot of complex **1**·THF and U(III) – U(VI) standards.

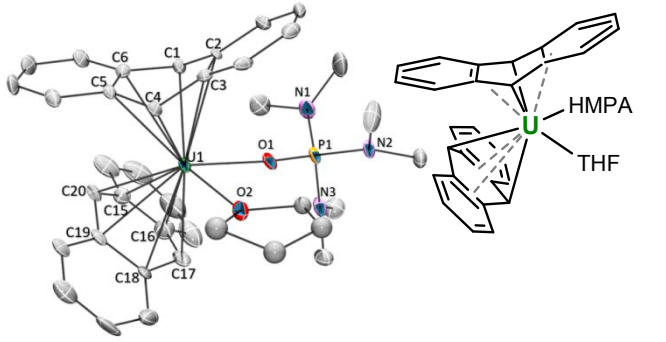

Fig. 4 ORTEP diagram of **3**·THF·C_6H_{14} with 30% thermal probability ellipsoids. Hydrogen atoms, co-crystallized THF and hexane are omitted for clarity.

^{1}H NMR spectrum of **1**·THF in THF-d_8 displays an excessively large HMPA resonance that can be attributed to the exchange of free and coordinated HMPA. However, recrystallization of **1**·THF from THF alone does not give way to the formation of **3**·THF·C_6H_{14}. It is possible that the Ag^+ cation may be acting as a Lewis acid, segregating the HMPA ligand; however, efforts to synthesize **3** using other Lewis acids (e.g., BPh_3) have not been successful. It is also possible that the transformation is light induced; however, no change is observed in standing solutions in ambient light. Moreover, all attempts to reproduce the synthesis of **3** using identical conditions have led to the sole isolation of **1**·THF. Nonetheless, the structural characterization of **3**·THF·C_6H_{14} reveals a novel reorganization that is not typically observed in arene-metalates.

The orientation of the two anthracenide rings in **3**·THF·C_6H_{14} exhibits a rotational offset of nearly 90° while maintaining a C_{cent}-U-C_{cent} = 134.1° bend angle comparable to **1**·THF. Inspection of the uranium-arenide contact distances reveals inequivalent interactions between the two anthracenides and uranium. On one hand, the coordination of ring 2 (C15 - C20) (Fig. 4) in **3**·THF·C_6H_{14} has similar features to those of **1**·THF, possessing a ring fold angle of 20.1° with accompanying distances of U1-C(ring1) = 2.527(9) – 2.854(9) Å (avg. 2.73 Å). On the other hand, the ligation mode of ring 1 (C1 – C6) (Fig. 4) may be better described as (η^2+η^4) or "slipped" η^6-binding,[14] due to two bonds being significantly longer than the others while still falling within the acceptable bonding range. Specifically, the U1-C2 = 2.932(8) Å and U1-C3 = 2.915(9) Å bonds fall outside of the 2.527(9) – 2.83(1) Å distances found for the other four U1-C(ring 1) bonds. However, these two longer bonds are still within the uranium-arene distances found in (η^6-C_6H_6)U($AlCl_4$)$_3$ (avg. U-C_{arene} = 2.91 Å).[15] Additionally, the bend angle of ring 1 is pronounced at 29.8°.

To probe for differences in the electronic structures between **1** and **3**, computational analyses were undertaken. Of note, DFT (PBE) geometries are in good agreement with experiment for both the ground state triplet and quintet states (Tables S5 to S6; see SI for DFT bond analysis). The electronic structure was further studied by multireference CASPT2 methods (see SI for details of active space choice). Energies for the CASPT2 ground state triplet were computed for all structures, and the CASPT2 energy is 3.2 and 2.9 kcal/mol lower for the quintet geometry than the triplet geometry in **1** and **3**, respectively (Table S7). Most notably, the CASSCF wavefunction changes when comparing the two spin-states (Fig. 5, Tables S8 and S9). In **1**, the electron configuration can be assigned as $\pi^{1.97}$ $\pi^{1.96}$ $\pi^{1.95}$ $\pi^{1.93}$ $5f^{1.00}$ $5f^{1.00}$ $\pi^{*0.05}$ $\pi^{*0.04}$ $\pi^{*0.03}$ $\pi^{*0.02}$ (where the superscript numbers are the CASSCF natural orbital occupation numbers) for the DFT triplet geometry. However, the CASSCF electron configuration is $\pi^{1.97}$ $\pi^{1.97}$ $\pi^{1.94}$ $\pi^{1.75}$ $5f^{0.99}$ $5f^{0.99}$ $\pi^{*0.24}$ $\pi^{*0.04}$ $\pi^{*0.05}$ $\pi^{*0.03}$ for the lower energy CASPT2 ground state triplet computed on the DFT quintet structure. Note that one set of π^* orbitals on the η^4-anthracene ligand is partially occupied. This is due to excitations from the bonding U-C interaction, labelled as π, to the corresponding antibonding orbital and not due to any reduction of spin in the uranium 5*f*-orbitals. These differences in π and π^* occupation can be expressed as a change in the radical character of the bond.[16] The CASPT2 calculation on the DFT triplet geometry has a bond with only 5% radical character due to partially occupying π^*, while the CASSCF result on the quintet structure has 24.5% radical character. Nevertheless, the CASSCF total spin density for both geometries is uranium-centred and consistent with a $5f^2$ configuration (Fig. S35). A similar trend occurs for **3**, although the π^* with partial occupation is on an η^6-anthracene ligand (Fig. S32). These results suggest that the CASSCF electronic structure is sensitive to geometry choice and that the distribution of spin in both **1** and **3** could be impacted by thermally accessible vibrational modes under experimental conditions.

Furthermore, CASPT2 calculations were performed on structures of **3** in which the U-C bond distances for this η^6-$C_{14}H_{10}$ ligand was varied (See SI for details, Table S10). Further elongating the bond with respect to the DFT quintet geometry increased the π^* occupation number while shortening reduced it. Although U-C bond distances were varied, on average from 2.690 Å to 2.858 Å, the total energy changed by less than 2 kcal/mol with respect to the fully optimized structure. The average experimental U-C distance falls within this range at 2.727 Å while the point that yielded the minimum CASPT2 energy has a bond distance of 2.774 Å. This suggests that the observed changes in spin-state geometries and electronic structures are sensitive to the molecular environment and may be affected by subtle factors such as crystal packing.

These analyses on **1** and **3**, combined with those determined

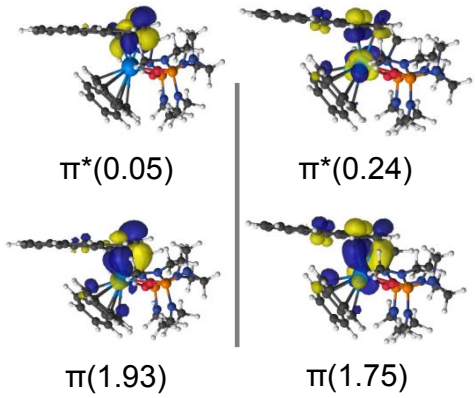

Fig. 5. Select CASSCF natural orbitals for **1** computed on the DFT triplet (left) and quintet (right) geometries (occupation numbers in parentheses).

for $\mathbf{A^{18C6}}$ and $\mathbf{A^{THF}}$, clearly show that these uranium-arenide complexes have electronic structures that are distinct from classical metallocenes and inverted sandwich complexes of the actinides, where the bonds typically comprise of a mix of σ, π, and δ-bonding.[8, 17] In our anthracenide compounds, the U-C bonds are exclusively π-type in character.

In conclusion, we have described the synthesis of the first neutral uranium-arenide sandwich complex, **1**·THF, from the reaction of **2** with 3 equiv. of $K[C_{14}H_{10}]$. Addition of the HMPA ligands appears crucial for the isolation of the mononuclear species. The redox non-innocence of the anthracene ligands combined with the redox activity of uranium prevents facile oxidation state assignments from X-ray structural parameters alone. Magnetic and XANES measurements supports a tetravalent assignment for the metal centre. In one instance, attempts to oxidize **1**·THF with AgOTf instead led to haptotropic ring rearrangement to give **3**·THF·C_6H_{14}, with both anthracenides displaying hexahapto coordination. DFT analyses on **1** and **3** show the latter to have a higher energy (+6.9 kcal/mol), implicating the AgOTf as a critical reagent for the observed ring migration. CASSCF computations reveal the uranium-arenide bonds to consist of π-type interactions. Interestingly, the CASSCF analyses show the triplet ground state on both the DFT-optimized triplet and quintet structures of **1** and **3** to be reasonable electronic models, where the difference in spin is not uranium-based but instead due to partial population of a U-C π*-orbital. Complexes **1** and **3**, along with $\mathbf{A^{18C6}}$ and $\mathbf{A^{THF}}$, are unprecedented arenide-actinide sandwich compounds that add to the long history of metal-arene complexes, thus presenting a one-of-a-kind molecular platform for further probing the reactivity and electronic properties of the early-actinide elements. Reactivity studies of these compounds are currently underway.

S.F. is grateful to the Welch Foundation (AH-1922-20200401), the NSF (DMR-1827745; CHE-1827875), and the Alfred P. Sloan Foundation for support of this work. This research used resources of the Advanced Photon Source under Contract No. DE-AC02-06CH11357. Computations were performed on High Performance Computing systems at the University of South Dakota (OAC-1626516). B. V. would like to thank the University of South Dakota for start-up funds. K. L. M. H. and M. M. are grateful for the support from the University of Ottawa, the Natural Sciences and Engineering Research Council of Canada, and the Canadian Foundation for Innovation.

Conflicts of interest

There are no conflicts to declare.

Notes and references

1. (a) H. Werner, *Angew. Chem. Int. Ed.*, 2012, **51**, 6052-6058; (b) H. L. Katja Heinze, *Organometallics*, 2013, **32**, 5623-5625.
2. V. M. Rayón and G. Frenking, *Organometallics*, 2003, **22**, 3304-3308.
3. (a) M. Rosillo, G. Domínguez and J. Pérez-Castells, *Chem. Soc. Rev.*, 2007, **36**, 1589-1604; (b) C. A. Merlic, M. M. Miller, B. N. Hietbrink and K. N. Houk, *J. Am. Chem. Soc.*, 2001, **123**, 4904-4918; (c) G. Pampaloni, *Coord. Chem. Rev.*, 2010, **254**, 402-419.
4. (a) D. M. Anderson, F. G. N. Cloke, P. A. Cox, N. Edelstein, J. C. Green, T. Pang, A. A. Sameh and G. Shalimoff, *J. Chem. Soc., Chem. Commun.*, 1989, 53-55; (b) J. G. Brennan, F. G. N. Cloke, A. A. Sameh and A. Zalkin, *J. Chem. Soc., Chem. Commun.*, 1987, 1668-1669; (c) F. G. N. Cloke, *Chem. Soc. Rev.*, 1993, **22**, 17-24.
5. R. P. Kelly, L. Maron, R. Scopelliti and M. Mazzanti, *Angew. Chem. Int. Ed.*, 2017, **56**, 15663-15666.
6. M. Dolg, *J. Chem. Inf. Model.*, 2001, **41**, 18-21.
7. J. Murillo, R. Bhowmick, K. L. M. Harriman, A. Gomez-Torres, J. Wright, R. W. Meulenberg, P. Miro, A. Metta-Magana, M. Murugesu, B. Vlaisavljevich and S. Fortier, *Chem. Sci.*, 2021, **12**, 13360-13372.
8. S. T. Liddle, *Coord. Chem. Rev.*, 2015, **293-294**, 211-227.
9. M. H. Jang and J. E. Ellis, *Angew. Chem. Int. Ed.*, 1994, **33**, 1973-1975.
10. M. Castillo, A. J. Metta-Magana and S. Fortier, *New. J. Chem.*, 2016, **40**, 1923-1926.
11. I. Korobkov, S. Gambarotta and G. P. A. Yap, *Angew. Chem. Int. Ed.*, 2003, **42**, 4958-4961.
12. D. R. Kindra and W. J. Evans, *Chem. Rev*, 2014, **114**, 8865-8882.
13. See Supporting Information for Details.
14. (a) M. A. Bennett, Z. Lu, X. Wang, M. Bown and D. C. R. Hockless, *J. Am. Chem. Soc.*, 1998, **120**, 10409-10415; (b) G. Zhu, K. E. Janak, J. S. Figueroa and G. Parkin, *J. Am. Chem. Soc.*, 2006, **128**, 5452-5461.
15. M. Cesari, U. Pedretti, Z. Zazzetta, g. Lugli and W. Marconi, *Inorg. Chim. Acta*, 1971, **5**, 439-444.
16. (a) K. Pierloot, H. L. Zhao and S. Vancoillie, *Inorg. Chem.*, 2010, **49**, 10316-10329; (b) W. Wu, J. T. De Hont, R. Parveen, B. Vlaisavljevich and W. B. Tolman, *Inorg. Chem.* , 2021, **60**, 5217-5223.
17. (a) N. Kaltsoyannis, P. J. Hay, J. Li, J.-P. Blaudeau and B. E. Bursten, in *The Chemistry of the Actinide and Transactinide Elements*, eds. L. R. Morss, N. M. Edelstein and J. Fuger, Springer Netherlands, Dordrecht, 2011, pp. 1893-2012; (b) R. J. Strittmatter and B. E. Bursten, *J. Am. Chem. Soc.*, 1991, **113**, 552-559; (c) B. E. Bursten and R. J. Strittmatter, *Angew. Chem. Int. Ed.*, 1991, **30**, 1069-1085.